

Lunar Radiation Environment and Space Weathering from the Cosmic Ray Telescope for the Effects of Radiation (CRaTER)

N. A. Schwadron^{1,2}, T. Baker^{1,2}, B. Blake³, A. W. Case⁴, J. F. Cooper⁵, M. Golightly^{1,2}, A. Jordan^{1,2}, C. Joyce¹, J. Kasper⁴, K. Kozarev^{4,6}, J. Mislinski^{1,2}, J. Mazur³, A. Posner⁷, O. Rother⁸, S. Smith^{1,2}, H. E. Spence^{1,2}, L. W. Townsend⁹, J. Wilson^{1,2}, and C. Zeitlin¹⁰

1. Space Science Center, University of New Hampshire, Durham, NH
2. Institute for the Study of Earth, Oceans, and Space, UNH, Durham, NH
3. The Aerospace Corporation, Los Angeles, CA
4. Harvard-Smithsonian Center for Astrophysics, Cambridge, MA
5. Heliospheric Physics Laboratory, NASA Goddard Space Flight Center, Greenbelt, MD
6. Department of Astronomy, Boston University, Boston, MA
7. NASA Headquarters, Washington, District of Columbia
8. Scientific Data Processing, Woltersweg 22, Kiel 24106
9. Department of Nuclear Engineering, University of Tennessee, Knoxville, TN
10. Space Science and Engineering Division, Southwest Research Institute, Boulder, CO

Corresponding Author: N. A. Schwadron (n.schwadron@unh.edu), Space Science Center, University of New Hampshire, 8 College Road, Durham, NH, 03824

Abstract

The Cosmic Ray Telescope for the Effects of Radiation (CRaTER) measures linear energy transfer by Galactic Cosmic Rays (GCRs) and Solar Energetic Particles (SEPs) on the Lunar Reconnaissance Orbiter (LRO) Mission in a circular, polar lunar orbit. GCR fluxes remain at the highest levels ever observed during the space age. One of the largest SEP events observed by CRaTER during the LRO mission occurred on June 7, 2011. We compare model predictions by the Earth-Moon-Mars Radiation Environment Module (EMMREM) for both dose rates from GCRs and SEPs during this event with results from CRaTER. We find agreement between these models and the CRaTER dose rates, which together demonstrate the accuracy of EMMREM, and its suitability for a real-time space weather system. We utilize CRaTER to test forecasts made by the Relativistic Electron Alert System for Exploration (REleASE), which successfully predicts the June 7th event. At the maximum CRaTER-observed GCR dose rate (~ 11.7 cGy/yr where Gy is a unit indicating energy deposition per unit mass, $1 \text{ Gy} = 1 \text{ J/kg}$), GCRs deposit ~ 88 eV/molecule in water over 4 billion years, causing significant change in molecular composition and physical structure (e.g. density, color, crystallinity) of water ice, loss of molecular hydrogen, and production of more complex molecules linking carbon and other elements in the irradiated ice. This shows that space weathering by GCRs may be extremely important for chemical evolution of ice on the Moon. Thus, we show comprehensive observations from the CRaTER instrument on the Lunar Reconnaissance Orbiter that characterizes the radiation environment and space weathering on the Moon.

1. Introduction.

Galactic Cosmic Rays (GCRs) and Solar Energetic Particles (SEPs) present formidable hazards for human exploration, mission and spacecraft operations. The Cosmic Ray Telescope for the Effects of Radiation (CRaTER) instrument on the Lunar Reconnaissance Orbiter (LRO) mission characterizes the global lunar radiation environment and its biological impacts by measuring GCR and SEP radiation behind a "human tissue-equivalent" plastic [Spence *et al.*, 2010]. CRaTER provides the fundamental measurements needed to test our understanding of the lunar radiation environment.

The current evolution of the Sun between solar cycles 23 and 24 remains highly anomalous compared to previous periods of the space age. The Sun has been abnormally quiet over a relatively long solar minimum when GCRs achieved the highest flux levels observed in the space age [Mewaldt *et al.*, 2010], and the power, pressure, flux and magnetic flux of solar wind were at the lowest levels [McComas *et al.*, 2008; Schwadron *et al.*, 2008; Connick *et al.*, 2011]. Even observations of the global heliosphere show remarkably rapid changes [McComas *et al.*, 2010] caused by dropping solar wind

pressure. This new period of solar evolution presents a unique opportunity to study the doses of GCRs when their fluxes remain at high levels. By relating GCRs to neutron fluxes observed from ground-based monitors and to GCR fluxes observed by other spacecraft such as Advanced Composition Explorer (ACE), we develop the capability to project GCR dose rates from the present period back through time when different interplanetary conditions prevailed.

Major advances made over the last decade in physics-based numerical modeling of the coupled Sun-to-Earth system now provide meaningful opportunities to use models in a predictive sense. Many agencies have prioritized predictive capabilities to serve their user communities [Spence *et al.*, 2004], including NOAA's Space Weather Prediction Center and NASA's Space Radiation Analysis Group at Johnson Space Center. An accurate warning system for SEP radiation hazards is critical in view of NASA's plans to send astronauts beyond low-Earth orbit. Demonstrating this commitment to the future of human exploration, NASA officially named the Multi-Purpose Crew Vehicle that could take its astronauts back to the moon, to Mars and to asteroids [see NASA, 2011].

However, space radiation remains a major factor for risk mitigation of safe deep space travel [Cucinotta *et al.*, 2010] and models of space radiation effects including dose and dose-equivalent rates remain largely untested.

CRaTER observations test predictions of the Earth-Moon-Mars Radiation Environment Module (EMMREM), a modeling project to develop and validate numerical modules for characterizing time-dependent radiation in the Earth-Moon-Mars and interplanetary space

environments [*Schwadron et al.*, 2010a]. EMMREM combines a suite of physics-based models that describe spatially varying and time-dependent ionizing radiation sources, including GCRs and SEPs, as well as the underlying heliospheric magnetic fields, plasmas, and transients which are important for the transport and access of these particles throughout the heliosphere. EMMREM incorporates the effects of primary particles, secondary radiation and dose calculations needed to compare with direct observations such as those provided by CRaTER.

The purpose of our paper is to test our understanding of the current lunar radiation environment, to utilize these models to project our understanding of the lunar radiation environment (due to GCRs) back through the space age, and develop tools that may be used to specify the radiation environment in near-real-time. In this vein, we test the viability of a new on-line system, (P)redictions of radiation from (R)EleASE, (E)MMREM, and (D)ata (I)ncorporating (C)RaTER, (C)OSTEP, and other (S)EP measurements (PREDICCS) at the University of New Hampshire. One component of the PREDICCS system runs the EMMREM model in real-time to provide dose calculations at the Earth, Moon and Mars starting in January of 2011.

PREDICCS also includes a new method for forecasting the radiation environment.

Posner [2007] showed how relativistic electrons provide up to ~1-hour advanced warning of the arrival time and intensity of the SEP ions. Observation of these relativistic electrons provides the basis for a real-time forecasting system called the Relativistic Electron Alert System for Exploration (REleASE) [*Posner*, 2009; Figure 1]. After one

year of operation at partner institutes at the Christian Albrechts University in Kiel, Germany and at NASA's (Community Coordinated Modeling Center) CCMC, REleASE showed sensitivity to relatively small events and yielded low false alarm rates. Here, we use CRaTER observations (SEP radiation dose) along with the REleASE model and the Comprehensive Suprathermal and Energetic Particle Analyzer (COSTEP) [*Muller-Mellin et al.*, 1995] observations from SOHO (which measures relativistic electrons) to verify, validate, and refine the model. The goal is to improve the reliability and thus value of the REleASE model toward realizing the up to 1-hour forecast of SEP events, a critical improvement over current forecasting.

(Figure 1)

In addition to the hazards they pose, GCRs are also an important energy source for space weathering, the general process of planetary surface and atmospheric modification by space environmental components including micrometeoroid bombardment, solar ultraviolet irradiation, solar wind and magnetospheric plasma, and more energetic charged and neutral particles including GCRs. The plasma-surface interaction processes [*Johnson*, 1990] can act to produce a thin layer of outer material covering and sometimes obscure the endogenic materials of greatest interest for understanding origins and interior evolution of the affected object. Within a series of weathered layers at increasing depth, products of GCR interactions extending to meter and greater depths may in turn be covered by other more highly processed products of lower energy particle interactions, and outermost layers may be eroded away by plasma and energetic ion sputtering.

Examples of weathered layers obscuring pristine ones are the radiation crusts [*Johnson et al.*, 1987] on cometary nuclei, also on Kuiper Belt and Oort Cloud Objects [*Moore et al.*, 2003; *Cooper et al.*, 2003; *Hudson and Moore*, 1999; *Hudson et al.*, 2008], and the iogenic components of sulfate hydrate deposits on the trailing hemisphere of Europa. In the latter case, near-infrared spectroscopy is used for mapping of the surface distributions [*McCord et al.*, 1998a,b, 1999, 2001; *Carlson et al.*, 1999, 2005; *Dalton et al.*, 2005; *Hibbits et al.*, 2000], as shown for the icy Galilean moons including Europa. Irradiation can make oxidants for life [*Chyba*, 2000; *Cooper et al.*, 2001] but also obscure and even destroy chemical signatures of prebiotic and potentially biological evolution that would otherwise be high priority targets on potentially habitable worlds such as Europa and Enceladus. Radiation-induced chemistry in surface ices, also called radiolysis, has even been proposed [*Cooper et al.*, 2009] as an energy source via magnetospheric electron irradiation for cryovolcanism on Enceladus and could contribute via GCR irradiation to outgassing activity on other icy surfaces including in the icy polar craters on the Moon. The long-term exposure throughout planetary regolith surfaces to meter depths depends largely on the doses caused by GCRs. Present progress on measuring evolution of GCR dose rates with CRaTER during the LRO mission is contributing to increased general understanding of the long-term effects of space weathering.

The paper is organized as follows. We relate GCR dose rates observed by CRaTER to predictions by EMMREM in Section 2. Observed and predicted doses from the June 7, 2011 SEP are compared in Section 3. Results from this event provide a blind test of the REleASE's predictive capabilities in Section 4. In the discussion (Section 5), we explore

implications of the CRaTER observations for the modulation of GCRs and space weathering at the Moon. Section 5 also compares CRaTER observations from the D1-D2 detector with previous CRaTER microdosimeter measurements [Mazur *et al.*, 2011] We conclude the paper in Section 6 by summarizing our current understanding of the lunar radiation environment, the potential use of EMMREM for determining radiation environment hazards, REleASE for forecasting, and the long-term implications of GCRs for space weathering.

2. Galactic Cosmic Ray Dose Rates.

We compare here the modeled doses from GCRs to data from CRaTER. GCR fluxes in EMMREM are based on a Local Interstellar Spectrum (LIS) of GCRs and the modulation potential [Badhwar and O'Neill, 1991; 1992; 1993; 1994; 1996], $\Phi = |Z e| \phi(r)$, where

$$\phi(r) = \int_r^{R_b} \frac{V(x)}{3\kappa_1(x)} dx \quad (1)$$

The integral in equation (1) extends from the inner solar system boundary at radius r to the outer modulation boundary R_b , the solar wind speed is $V(x)$ and $\kappa_1(x)$ is related to the radial diffusion coefficient, κ . The form for κ is based on a fit to the observed spectrum over time and species [O'Neill and Badhwar, 2006]: $\kappa = \kappa_1(r) P \beta$ where P is the rigidity in GV, β is the particle speed over the speed of light, $\kappa_1(r) \propto 1 + (r/r_0)^2$ and $r_0 = 4$ AU.

Reductions in the modulation potential are associated with enhanced diffusion, which causes higher fluxes of GCRs in the inner heliosphere.

The first of our three estimates of the modulation potential, Φ_{ACE} , (Figure 2, lower panel, blue curve) is derived by comparing the Bahdwar-O'Neil model with data from the Cosmic Ray Isotope Spectrometer (CRIS) on ACE. The modulation potential is adjusted to give the best overall fit to CRIS observations of differential energy fluxes for a variety of heavy GCR species (e.g., Oxygen).

(Figure 2)

The second estimate of the modulation potential is derived from McMurdo ground-based neutron monitor data (<ftp://ftp.bartol.udel.edu/>). Collisions between GCRs and atoms within Earth's atmosphere result in a cascade of secondary particles including neutrons that can be detected by ground-based monitors. Changes in neutron rates are small and proportional to the modulation potential based on linear expansion of the force-free solution of the Parker transport equation. A linear fit of the McMurdo count rate (MCR in 100's of counts per hour) to the ACE/CRIS modulation potential yields a new estimate for the modulation potential, $\Phi_{MCR} = -0.77 \times \text{MCR} + 8200$. The running 1-year average of Φ_{MCR} is shown in Figure 2 (red curve).

Interplanetary field dependence of the diffusion coefficient motivates a third estimate of the modulation potential, $\Phi_{|B|}$, based on the unsigned interplanetary magnetic field magnitude (ftp://nssdcftp.gsfc.nasa.gov/spacecraft_data/omni/omni_m_daily.dat). In this case, a power-law fit of the magnetic field to the ACE/CRIS modulation potential yields $\Phi_{|B|} = 35 |B(nT)|^{1.87} - 350$. This new field-based modulation potential provides an independent estimate of the modulation potential's evolution in time. In Figure 2 (green curve), we use 1-hour averages of the interplanetary field to provide an initial estimate of $\Phi_{|B|}$. We then form running 1-year averages ($\langle \Phi_{|B|} \rangle$) from the hourly data points. In the discussion section (§5.1), we show that this scaling of the modulation potential based on the interplanetary magnetic field strength is roughly consistent with a slab turbulence model of cosmic ray diffusion.

The modulation potentials $\langle \Phi_{|B|} \rangle$ and Φ_{MCR} agree well except for the period near 1970. All three modulation potentials track each other well from 1997 to 2007. However, after 2007, $\langle \Phi_{|B|} \rangle$ and Φ_{MCR} become significantly lower than Φ_{ACE} . Possible causes of the departure between these modulation potentials are discussed in §5.1.

Schwadron et al. [2010b] detailed the process by which modulation potentials are used in EMMREM to derive cosmic ray dose rates. The lens dose behind 0.22 g/cm^2 Al is an excellent proxy for the combined dose from the D1-D2 detector [*Spence et al.*, 2010] of the CRaTER instrument. Calculation of the dose is detailed in Appendix A. All dose rates shown here are referenced at the lunar surface (i.e., they are altitude-corrected) and are adjusted for dose deposition in water. We compare the dose rates using the three

estimates of the modulation potential with the CRaTER D1-D2 dose rates in the upper panel of Figure 2. All three modulation potentials generate dose rates that agree fairly well with CRaTER observations; however, Φ_{ACE} generates particularly good estimates of the dose rates.

Figure 3 focuses on the period in which CRaTER observations are available and compares dose observations (top) with the unsigned magnetic field measured near the Lagrangian point (L1; bottom). Much of the variability in the dose rates is associated with changes in the unsigned magnetic field. Preliminary analysis of the timescales of variability in the doses shows a noticeable 2-hour periodicity, consistent with the LRO spacecraft orbit period and eccentricity. This periodicity may be the result of local blockage by the Moon and associated GCR anisotropies.

(Figure 3)

In summary, the GCR doses observed by CRaTER generally agree well with model results from EMMREM. The dose rates peak at ~ 11.7 cGy/year, the highest dose rates observed in the space age.

3. Modeling Solar Energetic Particles

The Sun's slow evolution into solar cycle 24 has shown extremely low activity and very weak solar events. On June 7, 2011 (day-of-year 158), CRaTER observed one of the largest SEP events so far through the LRO mission. This event was still very small in comparison to historic events such as the Halloween 2003 storms [Schwadron *et al.*, 2010a]. In Figure 4, we compare EMMREM model predictions for dose rates during the June 7 event with observations from CRaTER. The EMMREM dose rates are applied for a lens dose proxy (1 g/cm² H₂O) with a 0.3 g/cm² Al shielding, which is comparable to the CRaTER D1-D2 detector (see Appendix A). The accumulated dose rate during the June 7 event (Figure 5) shows a total event dose of ~3 cGy, which is about two orders of magnitude smaller than the event dose of ~200-300 cGy during the Halloween storms. To place these doses into context, the 30-day radiation limit for short-term exposure to SEP events is 150 cGy skin dose and 100 cGy lens dose [Cucinotta *et al.*, 2010].

(Figure 4)

(Figure 5)

Table 1 shows a comparison between the EMMREM results and CRaTER observations both before and during the event. Prior to the event, the EMMREM dose rates are roughly 62% smaller than the CRaTER D1-D2 dose rates. This is explained by the fact that the BaRYon TRaNsport (BRYNTRN) model (a deterministic, coupled proton-neutron space radiation transport model that transports incident protons and their secondary products through shields of arbitrary composition and thickness; Wilson *et al.*,

1991) used here to determine dose rates takes into account only energetic protons, which contribute roughly half of the dose rate from GCRs. In contrast, SEP events are typically proton rich; therefore, during the SEP event, the agreement between EMMREM model results and observed dose rates significantly improves (the EMMREM dose during the SEP event is only 38% smaller than CRaTER D1-D2 observations). In fact, the EMMREM/CRaTER ratio may be diagnostic of the relative proton abundance in SEP events and GCR time series. Generally, results show excellent agreement, revealing that EMMREM can accurately determine the space radiation environment.

4. Forecasting Solar Energetic Particles

The PREDICCS system also incorporates REleASE, which uses 0.25-1 MeV relativistic electron data to provide proton flux forecasts for eight energy channels from 4 to 50 MeV. REleASE forecasts are based on empirical matrices that were fed during a training period of 1996-2002 with observed particle data. The matrix is filled with proton fluxes measured 30, 60 and 90 minutes later than the electron information (rise time and intensity). The advance warning time takes into account the approximate propagation time difference from the Sun to 1 AU between fast electrons and the much slower but more hazardous high-energy protons.

We utilize the forecast proton fluxes as inputs into the BRYNTRN model and the EMMREM model to provide predictions of the proton dose rates throughout the inner

heliosphere. Figure 6 shows the REleASE 60 minute forecast results at the Moon. The forecast from real-time data (blue points) shows that electrons of the incoming event have already started arriving at Day Of Year (DOY) 158.3, at about the same time as the arrival of the first protons of <40 MeV. However, the Deep Space Network (DSN) contact schedule did not allow measurement of the onset of the event earlier. The first increase of the proton forecast, as seen in archival REleASE forecast data (red points), started at DOY 158.277, more than 30 minutes prior to the arrival of the first protons. These results are encouraging for using REleASE for forecasting event onsets.

(Figure 6)

The actual doses from REleASE in Figure 6 have been plotted with arbitrary units since more work is needed to fully calibrate the REleASE inputs to EMMREM. The difficulty arises partly from the necessity to extrapolate energetic particle spectra from the relatively low energies provided by REleASE to higher energies (up to 2 GeV) that contribute more significantly to dose. Further, the proton energy spectrum unfolds from high to low energies due to proton propagation speed differences during the onset of SEP events. The elevated dose rates in the June 7th event arise largely from the increased energy of the roll-over in the energetic particle spectrum. Nonetheless, the REleASE dose predictions provide a succinct indicator of an approaching radiation hazard.

The REleASE model (blue points) has been run using near-real-time SOHO data downlinked from the DSN to specify the future evolution of SEPs. As a result, the only

predictions provided from REleASE are for periods when DSN transmissions are available. The data gaps occur when DSN is out of contact with the SOHO spacecraft. In contrast, the archival CRaTER data (black points) and archival SOHO/COSTEP proton observations (red points) have been compiled after the June 7 event to test the predictions of REleASE.

5. Discussion

The observations of dose rates observed by CRaTER have important implications for the modulation of GCRs (§5.1) and space weathering on the Moon (§5.2) and, by extension, to other all other airless, solar system objects. The estimates of dose from CRaTER's D1-D2 detector, as reported first here, are compared to CRaTER's micro-dosimeter observations [*Mazur et al.*, 2011] in (§5.3).

5.1 Modulation of Galactic Cosmic Rays in the Extended Cycle 23-24 Solar Minimum

Modulation of GCRs has caused the dose rates (Figures 2 and 3) to drop throughout much of the LRO mission. Observations of GCR dose rates, interplanetary magnetic field strengths and current sheet tilt angle (Figure 3) provide context for the effects of modulation discussed here.

The jumps in magnetic field strength observed near 2010.2 and 2011.2 (Figure 3, second panel) appear to be consistent with the sharp decreases observed in dose. Step-like

features have been analyzed in detail [Case *et al.*, 2010; Case, 2011]. The enhancements in the heliospheric magnetic field strength are due to closed magnetic flux fed into the heliosphere by Coronal Mass Ejections (CMEs) [Owens *et al.*, 2006, 2007; Schwadron *et al.*, 2008], which leads to increased modulation [e.g., Cliver and Ling., 2001]. Therefore, the reductions in GCR flux as solar activity increases are likely caused in part by increased interplanetary magnetic field strength associated with increased rates of CMEs.

The modulation potential $\langle \Phi_{|B|} \rangle$ depends almost quadratically on the interplanetary magnetic field strength, which is consistent with a relatively simple model of cosmic ray diffusion [le Roux *et al.*, 1999]. In this slab turbulence model, the parallel diffusion coefficient scales as $\kappa_{||} \propto r_g^2 / F^2$ where $r_g = pc/qB$ (p is momentum, c the speed of light, q is charge) is the cosmic ray gyroradius and $F = \delta B/B$ is the normalized (slab) component of interplanetary magnetic field fluctuations. The radial diffusion coefficient used in the modulation potential, equation (1), is given by $\kappa_{\perp} = (B_r/B)^2 \kappa_{||}$ where B_r is the radial magnetic field strength. If the normalized component of interplanetary field fluctuations F is roughly constant, then the radial diffusion coefficient scales with the inverse square of the interplanetary magnetic field strength, $\kappa_{\perp} \propto B^{-2}$, and the modulation potential scales with the square of the field strength, $\Phi \propto \kappa_{\perp}^{-1} \propto B^2$. This quadratic dependence of the modulation potential is similar to the power-law exponent of 1.87 inferred from the power-law fit of Φ_{ACE} to the interplanetary magnetic field magnitude.

The structure of the heliospheric magnetic field changes over the solar cycle. Near solar minimum, regions of uniform polarity emanate from the poles of the Sun. As activity

increases, the solar magnetic field becomes increasingly disordered and sources of magnetic flux migrate from the poles into the equatorial regions. Eventually, as the Sun evolves through solar maximum, magnetic flux migrates through the equatorial region and the polarity of the heliospheric magnetic field reverses [*Owens et al.*, 2007; *Schwadron et al.*, 2008]. Eventually as the Sun declines into the next solar minimum configuration, the reversed polarity fields coalesce into polar coronal holes and the heliospheric magnetic field again attains an ordered structure. This heliospheric magnetic field reversal process is likely driven through interchange reconnection between open magnetic flux and coronal mass ejections.

One parameter used to track the solar magnetic reversal process is the average tilt of the heliospheric current sheet (HCS). The HCS tilt angle also correlates with the relative magnitudes of drifts experienced by cosmic rays. Near solar minimum, the heliospheric current sheet is tilted only slightly from the equatorial plane, and the relatively ordered fields of the heliosphere cause strong cosmic ray drifts. However, nearer solar maximum these cosmic ray drift patterns break down [*Fisk and Schwadron*, 1995] as the current sheet becomes strongly tilted on average and the field becomes highly disordered. In the third panel of Figure 3, we show results from Potential Source Surface Models (e.g., from the Wilcox observatory, <http://wso.stanford.edu/>) for the tilt of the heliospheric current sheet. The current sheet was near the ecliptic in end of 2009 (~2009.75), about 3 months before the maximum in GCR dose rate was observed. The precipitous drop in GCR dose rate in 2010 and 2011 occurred as the current sheet rose to high latitudes, and the reversal in the heliospheric magnetic field is now occurring as of autumn 2011. There is about a

3-month delay between abrupt changes in the current sheet's inclination (2009.75 and 2010.9) and resulting drops in GCR dose rate (2010 and 2011.2). This delay may be caused by the propagation time of these field changes through the inner heliosphere, so the drops in GCR flux and dose rates are also likely associated with the changes of cosmic ray drifts in the evolving heliospheric magnetic field.

The elevated dose rates derived from the $\langle \Phi_{|B|} \rangle$ and Φ_{MCR} modulation potentials agree less favorably with CRaTER observations than those deduced from Φ_{ACE} . The cause for the departure between Φ_{MCR} and Φ_{ACE} in these modeled dose rates is a result of higher GCR proton fluxes compared to heavier GCR species such as oxygen, which have larger rigidities than protons. Multiple effects may contribute to the difference between the lower and higher rigidity GCR species:

- Deep in solar minima, three-dimensional drifts of cosmic rays become quite important [Jokipii *et al.*, 1977; Florinski *et al.*, 2003; Potgieter and le Roux, 1992]. GCR protons have drift paths that differ from higher rigidity GCRs.
- The reduced solar wind pressure [McComas *et al.*, 2008; Schwadron and McComas, 2008] in the deep cycle 23-24 solar minimum has allowed the termination shock to move closer to the Sun and resulted in a weakened modulation of the heliosheath [Scherer *et al.*, 2011]. Low rigidity GCR protons are more strongly modulated in the inner heliosheath. Therefore, higher GCR proton fluxes may penetrate the weakened heliosheath magnetic fields in the deep and extended cycle 23-24 minimum.

- The reduction in the interplanetary magnetic field strength to the lowest values of the space age [*Connick et al.*, 2010; *Schwadron et al.*, 2010] may preferentially enhance GCR protons. The magnitude and variance of the interplanetary magnetic field falls during solar minimum, which increases diffusion [e.g., *Wibberenz et al.*, 2002; *Manuel et al.*, 2011]. GCR protons are more sensitive to time-dependent changes in the interplanetary magnetic field strength because they have lower rigidity than heavier GCR species such as Oxygen. A sharp drop in the interplanetary magnetic field strength, like the one that occurred during the cycle 23-24 minimum, should significantly increase GCR proton fluxes while causing less pronounced increases in heavier GCRs species.

In summary, the dose rates observed by CRaTER reveal the importance of interplanetary magnetic field in regulating the diffusion of cosmic rays. The reduction of solar wind flux and pressure in the extended solar minimum between cycles 23 and 24 may weaken modulation by the inner heliosheath, which acts to preferentially increase the fluxes of GCR protons as compared to heavier species of cosmic rays.

5.2. Implications for Lunar Space Weathering

The alteration of ices by fast ions is observed in the laboratory [*Cheng and Lanzerotti*, 1978]. This form of irradiation breaks molecular bonds in the solid, which in turn produces new species that react with neighbors to form new molecules. On the Moon, space weathering has two major implications: first, space weathering causes the alteration

of any ice within the regolith; secondly, surfaces exposed to long-term space weathering will have reduced reflectance, as they become progressively red, grey and then black depending on the age of the surface and the average GCR fluxes to which these surfaces are exposed. A dominant molecular product is H₂, which can be lost from materials if it is sufficiently mobile [*Brown et al.*, 1987]. If molecular hydrogen is preferentially lost from a material or ice, the hydrogen-to-carbon ratio is driven down [*Lanzerotti et al.*, 1985; 1987]. The fate of H₂ from space weathering on the moon is an important topic that is being actively investigated by the LRO team. In this subsection, we describe implications of CRaTER observations for space weathering the regolith and the water ice it contains. The main question is whether CRaTER observes sufficiently high doses on the Moon to cause significant effects due to GCR bombardment. CRaTER directly addresses this question by providing the first observations of dose near the lunar surface.

We expect space weathering of matter to occur in a thin portion of the outer regolith of the Moon. Beam studies using lunar highland regolith simulant showed that 290 MeV/nucleon ¹⁰Be ions were attenuated after passage through about 25 g/cm² of regolith, which corresponds to ~15 cm depth assuming a regolith density of ~1.9 g/cm³ [*Miller et al.*, 2009]. Similarly, measurements and model calculations involving an array of heavy species indicate that a fairly small amount of soil (density of 1.4 g/cm³) with thickness of 46 cm or less attenuates the vast majority of GCR nuclei and solar proton event (SPE) protons, with only modest residual dose from surviving charged fragments of the heavy beam [*Miller et al.*, 2009]. In these cases, the bulk of energy deposition occurs for a column density of 22 g/cm². These results are fairly consistent, showing that GCRs are

attenuated and therefore cause the build-up of defects in a thin outer layer of regolith less than 50 cm.

The maximum dose rate observed by CRaTER D1-D2 corresponds to a deposition of ~ 22 eV/(molecule-Gyr) in ~ 1 g/cm² H₂O. (Here we take 1 molecule = 18 Atomic Mass Units, AMU). In the lunar regolith we are concerned with dose deposition in a column density ~ 20 g/cm². *Schwadron et al.* (2010b) showed doses in ~ 1 g/cm² H₂O are very similar (to within $\sim 5\%$) to doses in 10-20 g/cm² H₂O (skin versus blood forming organs in humans). Therefore, the D1-D2 H₂O dose observed by CRaTER is a good estimate of the dose in the water (ice) within the outermost regolith. It is difficult to estimate the true dose at the Moon over 4 billion years because the flux of GCRs is poorly known over the entire lunar history. However, examination of annual ¹⁰Be data (Julian calendar years 1428–1930; *McCracken et al.*, 2007) suggests that GCR fluxes during the space age were anomalously low in comparison to typical GCR fluxes over the last 600 years. As a result the CRaTER-based estimate of ~ 22 eV/(molecule-Gyr) may actually be a significant *underestimate* of the accumulated dose on the lunar surface. Therefore, over 4 billion years, it is likely that the lunar regolith was exposed to more than 88 eV/molecule.

Large changes in the local interstellar medium (LISM) may have dramatic effects on the heliosphere and its ability to modulate GCRs. Passage of the solar system through a typical enhancement (by a factor of 10) in the density of the LISM causes the entire heliosphere to shrink to about a quarter of its current size [*Zank and Frisch*, 1999], and increases the fluxes of GCRs at Earth by a factor of ~ 10 – 100 times for kinetic energies

below 100 MeV and 2–3 times in the interval 0.1–1 GeV [Scherer *et al.*, 2002]. The true form of the GCR spectrum in the LISM is unknown below a few GeV, but direct exposure to the full LISM spectrum [e.g., Cooper *et al.*, 2003, 2006] could result in even higher exposures at all such energies. Such changes in GCR fluxes are difficult to determine, making long-term estimates of the lunar dose highly uncertain.

At a dose of ~60 eV/molecule, an exposed surface will develop enough defects to alter its reflectance [Strazzulla *et al.*, 1988]. The dose is often expressed as a G-value (alterations/100 eV deposited). For example, water ice is altered ($2\text{H}_2\text{O} \rightarrow 2\text{H}_2 + \text{O}_2$) with $G \approx 0.7$ for α -particles and with $G \approx 0.3$ for β -particles [e.g., Hart and Platzman, 1961]. Carbon atoms in materials and ices tend to aggregate into larger molecules under ion bombardment [Moore *et al.*, 1983], and as carbon-containing species become linked, the reflectance changes, first becoming yellow or red, and then grey and possibly black depending on the mix of elements in a material and the total dose to which it is exposed [Piscitelli *et al.*, 1988, Khare *et al.*, 1989; Andronico *et al.*, 1987; Thompson *et al.*, 1987; Strazzulla *et al.*, 1984]. The dose for a material to blacken is ~100 eV/molecule and ~1000 eV/molecule for a material blacken. The CRaTER observed dose-rates indicate lunar surface exposure of more than 88 eV/molecule over 4 billion years, which implies that a permanently exposed surface would undergo significant reddening due to GCRs. These changes in reflectance contribute to other forms of reddening due to compositional changes such as submicroscopic iron accumulation due to solar wind sputtering and micrometeorite impact vaporization [Hapke, 2001].

Permanently shaded regions on the Moon should exhibit particularly strong effects from GCR bombardment due to the relative lack of other agents. Unlike more exposed regions of the lunar surface, permanently shaded regions are protected from sunlight, solar wind bombardment and UV exposure. This implies that permanently shaded regions are effective ice traps, and therefore important targets for future exploration. GCRs still have access to these sheltered regions, however, and GCR bombardment will cause the build-up of chemical alterations in the outer layers of the regolith there. Therefore, the upper ~50 cm layer of the regolith within permanently shaded regions could be subject to significant space weathering by GCRs, depending on the age of the surface. Based on CRaTER D1-D2 dose rates of $D_I=22$ eV/(molecule-Gyr) and with $G \approx 0.6$ /100 eV [Johnson, 1989], we find that the fraction of altered water ice is more than $1-\exp(-D_I GT) \approx 9\%$ in T=1 Gyr assuming no additional modifications to the regolith. This estimate demonstrates that GCRs on the Moon can significantly chemically modify ices in the regolith – particularly in permanently shaded craters.

The gardening process due to impacts of dust, comets and asteroids mixes the regolith and resupplies the lunar surface with ice in some cases. Solar wind, UV and SEPs also continually supply the surface with new elements, and erode and sputter material from the surface. Chemical alterations caused by GCRs should be considered along with other processes (solar wind, UV, impacts) that continually modify the regolith.

The radiation effects measured by CRaTER at the moon can be compared to other similar radiation environments throughout the solar system, particularly at airless bodies. For

example, we compare the CRaTER dose estimate with a dose estimate developed previously [Johnson, 1989] at Pluto. We consider the quantity D_M (eV/molecule) that represents the dose received by Pluto in a single orbit about the Sun (7.6×10^9 sec). The peak dose observed by CRaTER (11.7 cGy/year) integrated over one orbit by Pluto is $D_{M-CRaTER} = 5.3 \times 10^{-6}$ eV/molecule, which is about 1.7 times lower than the value of $D_M = 9 \times 10^{-6}$ eV/molecule found by Johnson [1989]. Note, however, that Johnson [1989] estimates GCR doses from an unmodulated GCR spectrum. On the bodies throughout the solar system including the Moon, direct exposure to the full LISM fluxes [Cooper et al., 2006] could occasionally produce much higher dose rates. Averaged over billions of years, a factor of 1.8 reduction in dose at the Moon due to modulation is quite reasonable. Therefore, our estimate based on CRaTER measurements is roughly consistent with the Johnson [1989] dose estimate. While the orbit-integrated dose on Pluto is quite small, the dose integrated over the age of Pluto is significant, which would cause reddening and darkening of the surface.

In summary, CRaTER provides direct observations of dose rates near the lunar surface. These CRaTER dose rates are likely underestimates of the average dose rates over long periods of time, implying dose deposition of more than 88 eV/molecule over 4 billion years. As a result, GCRs cause significant space weathering on the Moon. This is particularly the case in permanently shaded regions, which are bombarded by GCRs while being protected from visible light, UV, and solar wind. The exposure of material within these shaded regions should reduce reflectance, cause elevated carbon to hydrogen ratios, and lead to the build-up of significant chemical alteration within the outer regolith.

The large GCR dose rates observed by CRaTER suggest that GCR bombardment plays an important role in the balance that determines the amounts of water ice within regolith of permanently shaded craters.

5.3 Comparison between CRaTER D1-D2 dose rates and results from the micro-dosimeter

The estimates of dose from CRaTER D1-D2 are compared to results from the micro-dosimeter. *Mazur et al.* [2011] reported micro-dosimeter measurements of radiation dose from June 2009 through May 2010. They found that the micro-dosimeter rate was $\sim 6 \times 10^{-7}$ Rads/sec (18.9 cGy/year in Si) in June 20, 2009 when the LRO spacecraft was $\sim 10,000$ km from the Moon. During the same timeframe, D1-D2 dose rate *in Si* (recall from Appendix B that the dose rate in Si is 33% lower than in H₂O) projected to the lunar surface was ~ 8.3 cGy/year; at 10,000 km altitude, the D1-D2 dose rate is 16.5 cGy/year. There are some differences between the shielding of the microdosimeter (~ 1 g/cm² Al) and the D1-D2 detector (0.22 g/cm² Al). However, the GCR doses for these levels of shielding are quite similar [e.g., *Schwadron et al.*, 2010b]. The result is that CRaTER's measured D1-D2 Si dose rate (16.5 cGy/year) is $\sim 15\%$ lower than the micro-dosimeter dose rate (18.9 cGy/year). While these dose rates are similar, the difference suggests an absolute dose rate uncertainty of $\sim 15\%$.

6. Summary.

We utilize the EMMREM model to survey doses caused by GCRs throughout the space age including the recent period starting in mid-2009 when LRO/CRaTER observed the highest dose rates in the last half century, reinforcing the peculiarity of the deep solar minimum [e.g., *Mewaldt et al.*, 2010]. Agreement between model predictions and observations are excellent.

We report on one of the largest SEP events observed by CRaTER thus far in the LRO mission. The June 7th CRaTER event was quite small in comparison to historic events; for example, integrated doses were several orders of magnitude smaller than those achieved in the 2003 Halloween storms. The June 7th event presents an opportunity to compare results of EMMREM and REleASE forecasts of the event with CRaTER observations. The EMMREM results showed dose and dose-rates similar to those observed by CRaTER (1.9 cGy dose from EMMREM versus 3.0 cGy from CRaTER) demonstrating the viability of using EMMREM operationally for determination of hazards in the space radiation environment. The REleASE forecasts were successful at predicting the onset of the two rises of the June 7th CRaTER event. Our results reinforce the potential of the REleASE tool for prediction of event onsets.

In the case of bodies like the Moon that have no atmosphere, GCRs directly bombard and chemically alter and erode the regolith. For planets and moons with atmospheres, the increased GCR fluxes will cause elevated energy deposition in the atmosphere, heating, and possibly elevated atmospheric escape. It is shown that over 4 billion years at the

maximum CRaTER observed dose rate, GCRs deposit more than 88 eV/molecule into meters-deep lunar regolith. More exposed layers closer to the surface at micron to millimeter depths receive higher skin dosages but are also eroded away by solar ion sputtering and micrometeoroid impacts. The effects of space weathering by GCRs cause chemical alteration of water ice, loss of molecular hydrogen, and production of other molecular species due to interactions of the remaining oxygen with other elements such as carbon in the mixed ice. Lifetimes for survival of chemically recognizable organics, whether from abiotic or biotic sources, are limited by oxidation from long accumulation of GCR-induced oxidants in surface ices. GCR bombardment likely plays an important role in determining the amounts of non-chemically altered ice available within the regolith of permanently shaded craters.

Thus, we show comprehensive observations from the Cosmic Ray Telescope for the Effects of Radiation (CRaTER) on the Lunar Reconnaissance Orbiter (LRO) that characterize the lunar radiation environment. These results have important implications for space weathering. We compare CRaTER observations with EMMREM results and forecasts by REleASE that demonstrate the viability of using these tools to operationally characterize the lunar radiation environment in future exploration and mission operations.

Acknowledgements

This work is supported by the NASA CRaTER Contract NNG11PA03C and the EMMREM project, and for JFC by the NASA Lunar Advanced Science and Exploration Research and Outer Planets Research programs.

Appendix A. Calculation of the D1-D2 dose rate.

Each cosmic ray event in a CRaTER detector is digitized to an analog digital unit (ADU) channel value between 0 to 4095. The three thick detectors are subject to approximately the same conversion factors, and the three thin detectors have a different conversion factor. Laboratory calibrations showed that the channel-to-energy conversion can be expressed as:

$$\text{Deposited Energy} = E_0 + \text{channel} \{ \text{Gain} [1 + R (T - T_0)] \} \quad (1)$$

where T is the instrument temperature, Gain is the differential energy deposited per channel (keV/ADU) at temperature $T_0 = 22^\circ \text{C}$, R (keV/ADU/ $^\circ \text{C}$) is the sensitivity of the gain to temperature and E_0 (keV) is the energy deposited for channel zero. (ADU values below 7 are mostly electronics noise events, and are treated here as non-detections).

Table 2 lists these calibration coefficients.

Temperatures are typically in the range of 20° to -20°C , and given the small dependence (R) on temperature, we can closely approximate the relationship as:

$$\text{Deposited Energy} = E_0 + \text{channel} \times G \quad (2)$$

where $G' = 76.0$ keV/ADU for D1 and $G' = G = 21.8$ keV/ADU for D2. The absorbed dose is then the deposited energy divided by the mass of the detector, which is 0.332 g for D1 and 2.24 g for D2.

Linear energy transfer (LET) refers to energy lost per unit length in the detectors (detector thicknesses are 148 μm for D1 and 1000 μm for D2). Deposited dose typically spans a range of LETs including both the primary GCR and secondary particles that result from this primary. By combining the dose associated with both the thin and thick detector, we provide a definitive measurement of deposited dose. However, there is also the potential for double-counting dose contributions because D1 and D2 have overlapping LET coverage. By studying the LET spectra in these detectors, we find that the appropriate breaking point for LET between D1 and D2 is at 20.1 keV/ μm , which occurs in ADU 38 for D1 and ADU 920 for D2. The total dose deposited in the D1-D2 detectors is the sum of the dose from independent measurements in D1 (ADU range 38-4095) and from D2 (ADU range 7-920). If the same measurement results in both D1 and D2 deposited energies, then we take the deposited energy in D1 as the contributor to dose.

The LRO spacecraft is in a roughly circular polar orbit about the Moon. However, the altitude has varied from thousands to tens of thousands of km. The Moon represents an obstacle that blocks a portion of the incident cosmic rays. Near the lunar surface, the Moon blocks a portion of the incident GCRs. We use a correction factor, $1/[1 + \{1-$

$[R_m/(R_m+h)]^2\}^{1/2}$], that multiplies the dose-rate at mean altitude h to yield the dose-rate on the lunar surface (R_m is a lunar radius). This altitude adjusted dose is only applicable below ~1900 km where the moon blocks out a larger section of the sky than that intercepted by the nadir pointing stack of detectors, from D3 to D6, behind D1 and D2.

The CRaTER D1 and D2 detectors measure dose deposited in silicon. However, in order to estimate the radiation hazard to human organs (such as the lens) and in water ice on the Moon, we must inflate the Si dose by ~33% to yield the dose in water (see Appendix B). This altitude correction is used for the doses shown throughout the paper.

Appendix B. Calculation of the D1-D2 dose rate.

Many measurements of space radiation have been, and continue to be, made using silicon detectors. In many experiments, the quantities of interest are the fluxes of individual ion species in particular energy bins. Detectors and electronics are optimized accordingly.

ACE/CRIS provides a good example of this. In contrast, CRaTER is optimized to measure energy deposition distributions in silicon over a very wide dynamic range. These measurements must be converted to tissue dose. As in analysis done by other groups (e.g., Beaujean 2002) a single scaling factor is used to perform this conversion.

In principle, calculation of dose requires knowledge of the charge, mass, and energy of each incident particle in order to calculate its LET in water; the LET values of individual particles are multiplied by path length (detector thickness), summed and divided by the mass. In practice, we do not have this detailed information, so instead we add together all

the energy depositions in silicon and divide by the mass to get the dose in silicon. We then need to account for the difference in ionization potentials between silicon and water. The ionization potential appears in the logarithmic term in the Bethe-Bloch equation, and introduces energy dependence when the ratio of dE/dx in two materials is computed. At typical GCR energies of several hundred to a few thousand MeV/nuc, the ratio of dE/dx in the two materials is fairly constant. The lower ionization potential of water compared to silicon results in larger energy depositions per unit mass for a particle with a given charge and velocity. Careful study shows that for the GCR energy range of interest the ratio of dE/dx in silicon to dE/dx in water is about 1.75, an estimate that includes d-ray escape from finite depths of silicon. This also includes the effect of the higher density of silicon, which must be factored out, resulting in a multiplicative factor of 1.33 to be applied to the silicon dose. This can be seen from considering the sums over energy depositions, DE_i , in the two materials:

$$\frac{D_{water}}{D_{Si}} = \frac{\sum_i (\Delta E_i)_{water} / m_{water}}{\sum_i (\Delta E_i)_{Si} / m_{Si}} = \frac{\rho_{Si}}{\rho_{water}} \frac{\langle (\Delta E_i)_{water} \rangle}{\langle (\Delta E_i)_{Si} \rangle} = (2.33/1.75) = 1.33 \quad (2)$$

where D is dose, ΔE is energy deposited per event, m is the mass into which dose is deposited and ρ is mass density. The average energy deposited per unit volume is given by $\langle \Delta E \rangle = (1/A) dE/dx$ where A is effective detector area. The subscripts “water” and “Si” refer to the material into which energy is deposited. The energy dependence of the ratio introduces an uncertainty on this factor of about $\pm 5\%$, comparable to or smaller than other uncertainties in the measurement.

Acronyms

ACE	Advanced Composition Explorer
ADU	Analog Digital Unit
AMU	Atomic Mass Unit
AU	Astronomical Unit
BRYNTRN	Baryon Transport Model
CCMC	Community Coordinated Modeling Center
cGy	100 cGy = 1 Gy = 1 J/kg
CME	Coronal Mass Ejection
COSTEP	(Co)mprehensive (S)upra(t)hermal and (E)nergetic (P)article Analyzer
CRaTER	Cosmic Ray Telescope for the Effects of Radiation
CRIS	Cosmic Ray Isotope Spectrometer
DOY	Day Of Year
DSN	Deep Space Network
EMMREM	Earth Moon Mars Radiation Environment Module
eV	electron Volt
GCR	Galactic Cosmic Ray
GeV	10^9 electron Volts
HCS	Heliospheric Current Sheet
keV	10^3 electron Volts
L1	Lagrangian Point

LET	Linear Energy Transfer
LIS	Local Interstellar Spectrum
LISM	Local Interstellar Medium
LRO	Lunar Reconnaissance Orbiter
NOAA	National Oceanic and Atmospheric Administration
NASA	National Aeronautics and Space Administration
MCR	McMurdo neutron monitor
MeV	10^9 electron Volts
PFSS	Potential Field Source Surface
PREDICCS	(P)redictions of radiation from (R)EleASE (E)MMREM, and (D)ata (I)ncorporating (C)RaTER, (C)OSTEP, and other (S)EP measurements
Rad	1 cGy = 0.01 J/kg
REleASE	Relativistic Electron Alert System for Exploration
SEP	Solar Energetic Particle
SOHO	(So)lar and (H)eliospheric (O)bservatory
SPE	Solar Proton Event
UV	Ultraviolet

References

Andronico, G., G. A. Baratta, F. Spinella, and G. Strazzulla, Optical evolution of laboratory-produced organics - Applications to Phoebe, Iapetus, outer belt asteroids and cometary nuclei, *Astron. Astrophys.*, 184, 333, 1987.

Badhwar, G. D., and P. M. O'Neill (1991), An improved model of galactic cosmic radiation for space exploration missions, *Proc. Int. Conf. Cosmic Rays 22nd*, 1, 643–646.

Badhwar, G. D., and P. M. O'Neill (1992), An improved model of galactic cosmic radiation for space exploration missions, *Nucl. Tracks Radiat. Meas.*, 20, 403–410, doi:10.1016/1359-0189(92)90024-P.

Badhwar, G. D., and P. M. O'Neill (1993), Time lag of twenty two year solar modulation, *Proc. Int. Conf. Cosmic Rays 23rd*, 3, 535–539.

Badhwar, G. D., and P. M. O'Neill (1994), Long term modulation of galactic cosmic radiation and its model for space exploration, *Adv. Space Res.*, 14, 749–757, doi:10.1016/0273-1177(94)90537-1.

Badhwar, G. D., and P. M. O'Neill (1996), Galactic cosmic radiation model and its applications, *Adv. Space Res.*, 17, 7–17, doi:10.1016/0273-1177(95)00507-B.

R. Beaujean et al. (2002), Radiation Measurements, Volume 35, Issue 5, 433-438.

Brown, W.L., G. Foti, L.J. Lanzerotti, J.E. Bower and R.E. Johnson (1987), Delayed emission of hydrogen from ion bombardment of solid methane *Nucl. Inst. and Meth*

B19/20, 899-902.

Carlson, R. W., R. E. Johnson, and M. S. Anderson (1999), Sulfuric acid on Europa and the radiolytic sulfur cycle, *Science* 286, 97–99.

Carlson, R. W., *et al.* (2005), Distribution of hydrate on Europa: Further evidence for sulfuric acid hydrate, *Icarus* 177, 461-471.

Case, A. W., H. E. Spence, M. J. Golightly, J. C. Kasper, J. B. Blake, J. Mazur, L. Townsend, and C. Zeitlin (2010), Variations in the Galactic Cosmic Ray Flux at the Moon: Effects of the Magnetotail and Solar Wind Structures, *Lunar and Planetary Institute Science Conference Abstracts*, 41, 2606.

Case, A. W. (2011), Galactic cosmic ray variations at the moon, Ph.D. Thesis, Boston University

Cheng, A.F. and L.J. Lanzerotti, (1978), Ice sputtering by radiation belt protons in the rings of Saturn and Uranus, *J. Geophys. Res.*, 83, 2597- 2602.

Chyba CF. (2000), Energy for microbial life on Europa, *Nature*, 403, 381-382.

Cliver, E. W. and A. G. Ling (2001), Coronal Mass Ejections, Open Magnetic Flux, and Cosmic-Ray Modulation, *Astrophys. J.*, 556, 432, doi: 10.1086/3215702001

Connick, D. E., C. W. Smith, and N. A. Schwadron (2011), Interplanetary Magnetic Flux Depletion During Protracted Solar Minima, *Astrophys. J.*, 727, 8, doi:10.1088/0004-637X/727/1/8.

Cooper, J. F., R. E. Johnson, B. H. Mauk, H. B. Garrett, and N. Gehrels (2001), Energetic Ion and Electron Irradiation of the Icy Galilean Satellites, *Icarus*, 149, 133-159.

Cooper, J. F., E. R. Christian, J. D. Richardson, and C. Wang (2003), Proton irradiation of Centaur, Kuiper Belt, and Oort Cloud Objects at Plasma to Cosmic Ray Energy, *Earth, Moon, and Planets*, 92, 261-277.

Cooper, J. F., M. E. Hill, J. D. Richardson, and S. J. Sturmer (2006), Proton irradiation environment of solar system objects in the heliospheric boundary regions, in *Physics of the Inner Heliosheath, Voyager Observations, Theory, and Future Prospects*, 5th Annual IGPP International Astrophysics Conference. AIP Conference Proceedings, edited by J. Heerikhuisen, V. Florinski, G.P. Zank and N.V. Pogorelov, AIP, Vol. 858, 372-379.

Cooper, J. F., P. D. Cooper, E. C. Sittler, S. J. Sturmer, and A. M. Rymer (2009), Old Faithful model for radiolytic gas-driven cryovolcanism at Enceladus, *Planetary and Space Science* 57, 1607-1620.

Cucinotta, F. A., S. Hu, N. A. Schwadron, K. Kozarev, L. W. Townsend, and M.-H. Y. Kim (2010), Space Radiation Risk Limits and Earth-Moon-Mars Environmental Models, *Space Weather*, 8, doi:10.1029/2010SW000572.

Dalton, J. B., *et al.* (2005). Spectral comparison of heavily hydrated salts with disrupted terrains on Europa, *Icarus*, 177, 472-490.

Fisk, L. A. and Schwadron, N. A. (1995), The influence of intermediate-scale variations in the heliospheric magnetic field on the transport of galactic cosmic rays, *J. Geophys. Res.*, 100, 7865.

Florinski, V., G. P. Zank, and N. V. Pogorelov (2003), Galactic cosmic ray transport in the global heliosphere, *J. Geophys. Res.*, 108(A6), 1228, doi:10.1029/2002JA009695.

Hapke, B., Space weathering from Mercury to the asteroid belt (2001), *J. Geophys. Res.*, 106, 10,039.

Hart, E. J. and R. L. Platzman (1961), Radiation Chemistry in Physical Mechanisms in Radiation Biology 1. (Academic Press, N.Y.), 93-120.

Hibbitts, C. A., T. B. McCord, and G. B. Hansen (2000), Distributions of CO₂ and SO₂ on the surface of Callisto, *J. Geophys. Res.*, *105*, 22541-22557.

Hudson, R. L. and M. H. Moore (1999), Laboratory Studies of the Formation of Methanol and Other Organic Molecules by Water+Carbon Monoxide Radiolysis: Relevance to Comets, Icy Satellites, and Interstellar Ices, *Icarus*, *140*, 451.

Hudson, R. L., M. E. Palumbo, G. Strazzulla, M. H. Moore, J. F. Cooper, and S. J. Sturmer (2008), Laboratory Studies of the Chemistry of TNO Surface Materials, in *The Solar System Beyond Neptune*, edited by A. Barucci, H. Boehnhardt, D. P. Cruikshank, and A. Morbidelli, 507-523, Univ. of Arizona Press, Tucson.

Johnson, R. E., J. F. Cooper, L. J. Lanzerotti, and G. Strazzulla (1987), Radiation Formation of a Non-Volatile Comet Crust, *Astronomy and Astrophysics*, *187*, 889.

Johnson, R. E. (1989), Effect of irradiation on the surface of Pluto, *Geophys. Res. Lett.*, *16*, 1233.

Johnson, R. E. (1990), Energetic charged-particle interactions with atmospheres and surfaces., *Physics and Chemistry in Space*, *19*.

Jokipii, J. R., E. H. Levy, and W. B. Hubbard (1977), Effects of particle drift on cosmic-

ray transport. I: General properties, application to solar modulation, *Astrophys. J.*, 213, 861.

Khare, B. N., W. R. Thompson, B. G. Murray, C. F. Chyba, C. Sagan, and E. T. Arakawa (1989), Solid organic residues produced by irradiation of hydrocarbon-containing H₂O and H₂O/NH₃ ices - Infrared spectroscopy and astronomical implications, *Icarus*, 79, 350.

Lanzerotti, L.J., W.L. Brown and R.E. Johnson (1985), Laboratory studies of ion irradiation of water, sulfur dioxide, and methane ices. in *Ices in The Solar System*, (eds. J. Klinger) (D. Reidel, Dordrecht), 317-331.

Lanzerotti, L.J., W.L. Brown, and K.J. Marcantonio (1987), Experimental study of the erosion of methane ice by energetic ions, *Astrophys. J.* 313, 910-919.

le Roux, J. A., G. P. Zank, and V. S. Ptuskin (1999), An evaluation of perpendicular diffusion models regarding cosmic ray modulation on the basis of a hydromagnetic description for solar wind turbulence, *J. Geophys. Res.*, 1042, 24845, doi: 10.1029/1999JA900318.

Manuel, R., Ferreira, S. E. S., Potgieter, M. S., Strauss, R. D., and Engelbrecht, N. E., Time-dependent cosmic ray modulation, *Adv. Space Res.*, 47, 1529, doi: 10.1016/j.asr.2010.12.007 2011.

Mazur, J. E., Crain, W. R., Looper, M. D., Mabry, D. J., Blake, J. B., Case, A. W., Golightly, M. J., Kasper, J. C., and Spence, H. E. (2011), New measurements of total ionizing dose in the lunar environment, *Space Weather*, *90*, 7002, doi: 10.1029/2010SW000641.

McComas, D. J., R. W. Ebert, H. A. Elliott, B. E. Goldstein, B. E., J. T. Gosling, N. A. Schwadron, and R. M. Skoug, Weaker Solar Wind from the Polar Coronal Holes and the Whole Sun (2008), *Geophys. Res. Lett.*, *35*, L18103, doi:10.1029/2008GL034896.

McComas, D. J., M. Bzowski, P. Frisch, G. B. Crew. M. A. Dayeh, R. DeMajistre, H. O. Funsten, S. A. Fuselier, M. Gruntman, P. Janzen, M. A. Kubiak, G. Livadiotis, E. Möbius, D. B. Reisenfeld, and N. A. Schwadron (2010), Evolving outer heliosphere: Large-scale stability and time variations observed by the Interstellar Boundar Explorer, *J. Geophys. Res.*, *115*, 9113, doi:10.1029/2010JA015569.

McCord, T. B., et al. (1998a), Salts on Europa's surface detected by Galileo's Near Infrared Mapping Spectrometer, *Science* *280*, 1242–1245.

McCord, T. B., et al. (1998b), Non-water-ice constituents in the surface material of the icy Galilean satellites from the Galileo near-infrared mapping spectrometer investigation, *J. Geophys. Res.* *103*, 8603–8626.

McCord, T. B., et al. (1999), Hydrated salt minerals on Europa's surface from the Galileo near-infrared mapping spectrometer (NIMS) investigation, *J. Geophys. Res.* *104*, 11827–11851.

McCord, T. B., et al. (2001), Thermal and radiation stability of the hydrated salt minerals epsomite, mirabilite, and natron under Europa environmental conditions, *J. Geophys. Res.* *106*, E2, 3311- 3319.

Mewaldt, R. A., A. J. Davis, K. A. Lave, R. A. Leske, E. C. Stone, M. E. Wiedenbeck, W. R. Binns, E. R. Christian, A. C. Cummings, G. A. de Nolfo, M. H. Israel, A. W. Labrador, T. T. von Rosnevinge, Record-setting Cosmic-ray Intensities in 2009 and 2010 (2010), *Astrophys. J. Lett.*, *723*, L1, doi: 10.1088/2041-8205/723/1/L1.

Miller, J., L. Taylor, C. Zeitlin, L. Heilbronn, S. Guetersloh, M. DiGiuseppe, Y. Iwata, T. Murakami, Lunar soil as shielding against space radiation (2009), *Radiation Measurements* doi:10.1016/j.radmeas.2009.01.010, *44*, 163-167.

Moore, M. H., B. Donn, R. Khanna, and M. F. A'Hearn (1983), Studies of proton-irradiated cometary-type ice mixtures, *Icarus*, *54*, 388.

Moore, M. H., R. L. Hudson, and R. F. Ferrante (2003), Radiation Products in Processed Ices Relevant to Edgeworth-Kuiper-Belt Objects, *Earth Moon and Planets*, *92*, 291.

Muller-Mellin, R., et al. (1995), COSTEP---Comprehensive suprathermal and energetic particle analyser, *Sol. Phys.*, 162, 483--504.

NASA, Preliminary Report Regarding NASA's Space Launch System and Multi-Purpose Crew Vehicle Pursuant to Section 309 of the NASA Authorization Act of 2010 (P.L. 111-267), January, 2011

O'Neill, P. M. (2006), Badhwar-O'Neill galactic cosmic ray model update based on Advanced Composition Explorer (ACE) energy spectra from 1997 to present, *Adv. Space Res.*, 37, 1727.

Owens, M. J., and N. U. Crooker (2006), Coronal mass ejections and magnetic flux buildup in the heliosphere, *J. Geophys. Res.*, 111, A10104, doi:10.1029/2006JA011641.

Owens, M. J., N. A. Schwadron, N. U. Crooker, W. J. Hughes, H. E. Spence (2007), The role of coronal mass ejections in the evolution and reversal of the coronal and heliospheric magnetic fields over the solar cycle, *Geophys. Res. Lett.*, 34, doi 10.1029/2006GL028795, 6104.

Piscitelli, J. R., D. P. Cruikshank, and J. F. Bell, (1988), Laboratory studies of irradiated nitrogen-methane mixtures - Applications to Triton, *Icarus*, 76, 118.

Posner, A. (2007), Up to 1-hour forecasting of radiation hazards from solar energetic ion

events with relativistic electrons, *Space Weather*, Vol. 5, doi: 10.1029/2006SW000268.

Potgieter, M. S., and J. A. le Roux (1992), The simulated features of heliospheric cosmic-ray modulation with a time-dependent drift model. I—General effects of the changing neutral sheet over the period 1985–1990, *Astrophys. J.*, 386, 336–346, doi:10.1086/171020.

Scherer, K., H. Fichtner, R. D. Strauss, S. E. S. Ferreira, M. S. Potgieter, and H.-J. Fahr (2011), On Cosmic Ray Modulation beyond the Heliopause: Where is the Modulation Boundary?, *Astrophys. J.*, 735, 128, doi: 10.1088/0004-637X/735/2/128.

Schwadron, N. A., M. Owens, and N. U. Crooker (2008), The heliospheric magnetic field over the Hale cycle, *Astrophys. Space Sci. Trans.*, 4, 19.

Schwadron, N. A. and D. J. McComas (2008), The Solar Wind Power from Magnetic Flux, *Astrophys. J. Letters*, 686, L33-L36.

Schwadron, N. A., L. Townsend, K. Kozarev, M. A. Dayeh, F. Cucinotta, M. Desai, M. Golightly, D. Hassler, R. Hatcher, M.-Y. Kim, A. Posner, M. PourArsalan, H. E. Spence, and R. K. Squier (2010a), Earth-Moon-Mars Radiation Environment Module framework, *Space Weather*, Vol. 8, doi:10.1029/2009SW000523.

Schwadron, N. A., A. J. Boyd, K. Kozarev, M. Golightly, H. Spence, , L. Townsend, and M. Owens (2010b), Galactic cosmic ray radiation hazard in the unusual extended solar minimum between solar cycles 23 and 24, *Space Weather*, Vol. 8, doi:10.1029/2009SW000567.

Schwadron, N. A., D. E. Connick, and C. Smith (2010c), Magnetic Flux Balance in the Heliopause, *Astrophys. J. Lett.*, doi: 10.1088/2041-8205/722/2/L132, 722.

Spence, H. E., D. Baker, A. Burns, T. Guild, C.-L. Huang, G. Siscoe, and R. Weigel (2004), CISM metrics plan and initial model validation results, *J. Atmos. Sol. Terr. Phys.*, 66, 1499-1507.

Spence, H. E., A. W. Case, M. J. Golightly, T. Heine, B. A. Larsen, J. B. Blake, P. Caranza, W. R. Crain, J. George, M. Lalic, A. Lin, M. D. Looper, J. E. Mazur, D. Salvaggio, J. C. Kasper, T. J. Stubbs, M. Doucette, P. Ford, R. Foster, R. Goeke, D. Gordon, B. Klatt, J. O'Connor, M. Smith, T. Onsager, C. Zeitlin, L. W. Townsend, and Y. Charara (2010), CRaTER: The Cosmic Ray Telescope for the Effects of Radiation Experiment on the Lunar Reconnaissance Orbiter Mission, *Space Science Reviews*, 140, 243-284.

Strazzulla, G., L. Torrioni, and G. Foti (1988), Light scattering from ion-irradiated frozen gases, *Europhysics Letters*, 7, 431.

Strazzulla, G., L. Calcagno, and G. Foti (1984), Build up of carbonaceous material by fast protons on Pluto and Triton, *Astron. Astrophys.*, *140*, 441.

Thompson, W. R., B. G. J. P. T. Murray, B. N. Khare, and C. Sagan (1987), Coloration and darkening of methane clathrate and other ices by charged particle irradiation: Applications to the outer solar system, *J. Geophys. Res.*, *921*, 14933.

Wibberenz, G., I. G. Richardson, and H. V. Cane, A simple concept for modeling cosmic ray modulation in the inner heliosphere during solar cycles 20-23 (2002), *J. Geophys. Res. (Space Physics)*, *107*, 1353, doi: 10.1029/2002JA009461.

Wilson, J. W., L. W. Townsend, W. S. Schimmerling, G. S. Khandelwal, F. S. Khan, J. E. Nealy, F. A. Cucinotta, L. C. Simonsen, J. L. Shinn, and J. W. Norbury (1991), Transport methods and interactions for space radiations, NASA Tech. Rep., 1257.

Table 1. Comparison between CRaTER and EMMREM results for the June 7 event

	Prior to Event (5/12 – 6/4)	June 7, 2011 CRaTER event (6/5 – 6/10)
CRaTER D1-D2 (cGy)	0.68	3.0
EMMREM (cGy)	0.26	1.9
CRaTER/EMMREM	2.6	1.6

Table 2. Calibration coefficients for energy conversion in D1 and D2

	E_0 (keV)	Gain (keV/ADU)	$R \times 100,000$ (keV/ADU/° C)
D1	105.1	76.3	19.31
D2	50	21.8	2.460

Figure 1: (top) from *Posner et al.* (2009) conceptually showing how relativistic electrons racing ahead of SEP ions provide an early warning of the radiation hazard to follow up to 90 minutes later. Schematic (lower panels) from *Schwadron et al.* [2010a] motivating EMMREM, which provides a suite of numerical modules to characterize time-dependent radiation exposure from the hazards posed by space radiation from (bottom left) flares and (bottom right) particles accelerated at CME shocks.

Figure 2. The modulation parameter (lower panel) based on observations of neutrons using McMurdo data (red), interplanetary magnetic field (green) and based on the Advanced Composition Explorer (ACE) Cosmic Ray Isotope Spectrometer (CRIS) measurements [blue; see O’Neil, 2006]. The modulation potentials are used via EMMREM to infer GCR lens dose rates. Dose rates deduced from EMMREM are shown (upper panel) as well as measurements from CRaTER’s D1-D2 detectors (black curve). The CRaTER D1-D2 dose rates were altitude adjusted to the lunar surface, have been adjusted for dose deposition in water (these dose rates), and represent two-week averages with SEP events removed. The polarity of the large-scale solar magnetic field is indicated by A : for $A > 0$ the Sun’s large-scale northern polarity is positive. The periods indicated by r show when field reversals occurred. Dose rates observed by CRaTER (black points in upper panel and upper right inset) near the highest dose levels during the space age. The solar images on the bottom panel show conditions of the corona (first and third

images from left) and photosphere (second and fourth image from left) near solar maximum (left two images) and solar minimum (right two images).

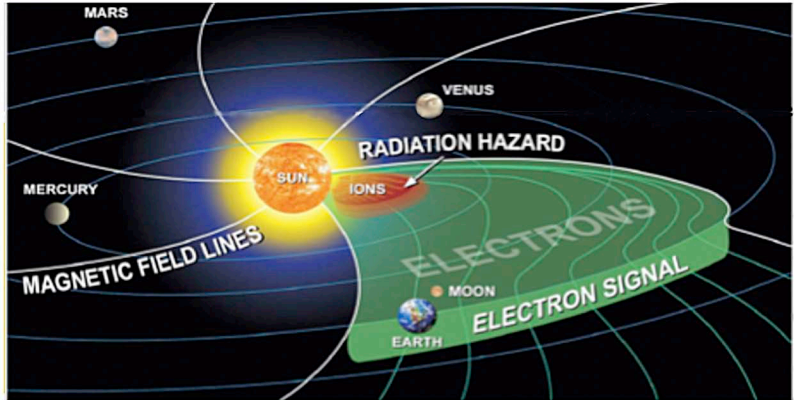
Figure 3. Comparison of dose observations by CRaTER D1-D2 detectors (upper panel) for GCR against model predictions from EMMREM (as detailed in Figure 2). Also shown (middle-panel) is the unsigned magnetic field magnitude. Time periods associated with SEP events are removed. Color-coding of model predictions are the same as in Figure 2. In the top panel, 1-hour averages from LRO/CRaTER are shown in purple, the light blue curve shows the running two-week average, and the black curves show the standard deviation from this running average. Similarly, in the second panel, the grey line shows the one-hour average of the unsigned magnetic field, with the green and black lines representing the running two-week average and the standard deviation, respectively. In the third panel, data from the Wilcox Solar Observatory (<http://wso.stanford.edu>) are shown for the tilt of the heliospheric current sheet (third panel). The classic Potential Field Source Surface (PFSS) model uses a line-of-sight boundary condition at the photosphere and includes a polar field correction. A newer model (Radial $R_s=3.25$) uses a radial boundary condition at the photosphere, a higher source surface radius (3.25 solar radii) and requires no polar field correction.

Figure 4. Comparison between EMMREM and CRaTER showing excellent agreement for dose rate. Observations from GOES at energy levels [0.74-4.2, 4.2-8.7, 8.7-14.5, 15-40, 38-82, 84-200, 110-900] MeV are fed into BRYNTRN on a 5-minute basis and used as the boundary conditions for characterizing the radiation environment throughout the

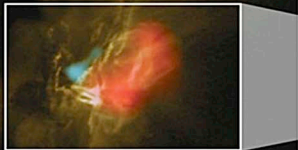
inner heliosphere [Schwadron *et al.*, 2010a]. Observations are both fed directly into BRYNTRN (red curves) and utilized as input within the EMMREM framework (blue curves) allowing propagation throughout the inner heliosphere. We show both the progression of the doses over a month (upper panel) and over a 5-day period focused on the June 7th event (lower panel).

Figure 5. The accumulated dose during the June 7, 2011 CRaTER event. The final dose for the June 7th, 2011 event is ~2 cGy, much smaller than historic events that typically reveal 100's of cGy. The agreement between modeled and observed doses is excellent. The small offsets between data values at the start of DOY 156 are due to differences in the resolution of the different data sources.

Figure 6. Results of the 60-minute REleASE forecast in comparison to CRaTER observations at the Moon. As in Figure 5, REleASE results are fed directly into BRYNTRN (red and blue points) and are fed into the EMMREM model so that they may be integrated throughout the inner heliosphere. Shown are forecast data from REleASE (blue; issued 60 minutes prior to events) and the archival data (red) generated after the event occurred. REleASE successfully predicts both components of the event.



SOLAR FLARE



CORONAL MASS EJECTION

